



# Process development and coaxial sensing in fiber laser welding of 5754 Al-alloy

Cite as: J. Laser Appl. **31**, 022419 (2019); <https://doi.org/10.2351/1.5096101>

Submitted: 14 March 2019 . Accepted: 14 March 2019 . Published Online: 29 April 2019

Matteo Garavaglia, Ali Gökhan Demir , Stefano Zarini, Brian M. Victor, and Barbara Previtali 



View Online



Export Citation



CrossMark

## ARTICLES YOU MAY BE INTERESTED IN

[Novel approach for weld depth determination using optical coherence tomography measurement in laser deep penetration welding of aluminum and steel](#)

Journal of Laser Applications **31**, 022007 (2019); <https://doi.org/10.2351/1.5082263>

[Estimation of melt pool size by complementary use of external illumination and process emission in coaxial monitoring of selective laser melting](#)

Journal of Laser Applications **31**, 022305 (2019); <https://doi.org/10.2351/1.5096117>

[Investigations on in-process control of penetration depth for high-power laser welding of thick steel-aluminum joints](#)

Journal of Laser Applications **31**, 022418 (2019); <https://doi.org/10.2351/1.5096105>



# Process development and coaxial sensing in fiber laser welding of 5754 Al-alloy

Cite as: J. Laser Appl. 31, 022419 (2019); doi: 10.2351/1.5096101

Submitted: 14 March 2019 · Accepted: 14 March 2019 ·

Published Online: 29 April 2019



View Online



Export Citation



CrossMark

Matteo Garavaglia,<sup>1</sup> Ali Gökhan Demir,<sup>1,a)</sup> Stefano Zarini,<sup>2</sup> Brian M. Victor,<sup>3</sup> and Barbara Previtali<sup>1</sup>

## AFFILIATIONS

<sup>1</sup>Department of Mechanical Engineering, Politecnico di Milano, Via La Masa 1, 20156 Milan, Italy

<sup>2</sup>Optoprim S.r.l., Via Carlo Rota 37, 20900 Monza, Italy

<sup>3</sup>nLIGHT, Inc., 5408 NE 88th Street, Building E, Vancouver, Washington 98665

**Note:** This paper is part of the Special Collection: Proceedings of the International Congress of Applications of Lasers & Electro-Optics (ICALEO® 2018).

<sup>a)</sup>**Author to whom correspondence should be addressed; electronic mail:** [aligokhan.demir@polimi.it](mailto:aligokhan.demir@polimi.it)

## ABSTRACT

The use of Al-alloys is increasing in the automotive industry due to the pressing necessity to reduce weight and fuel consumption. Several parts concerning the car body are assembled through welding, where a high-quality seam is a key requirement. For this purpose, laser welding stands as an appealing option. On the other hand, laser welding of Al-alloys is a complex process due to the high reflectivity, reactivity, and crack susceptibility of these materials. In many cases, such issues limit the applicability of the autogeneous welding, which is an advantageous feature of laser welding. High-brilliance fiber lasers have been an enabling technology for improving the weldability of Al-alloys. However, laser welding of Al-alloys, especially in a lap-joint configuration, requires robust processing conditions able to maintain seam quality for each weld in high volumes even with part tolerances and tooling variability. Accordingly, this work discusses the process development and monitoring in laser welding of 5754 Al-alloy. In particular, the process was carried out in a double lap-joint configuration with 1 mm sheets, commonly used in automotive applications. A 3 kW fiber laser with in-source integrated monitoring capability was employed as the light source. The process feasibility zone was investigated as a function of laser power and welding speed, while the effect of focal position was investigated for the weld robustness. Weld seam types and defects were identified, as well as the monitoring signals associated light back-reflected from the process.

**Key words:** keyhole welding, Al-alloy, double lap-joint, back reflection, remote sensing

© 2019 Laser Institute of America. <https://doi.org/10.2351/1.5096101>

## I. INTRODUCTION

In the last few years, the importance of aluminum and its alloys has been growing in many industrial sectors and for many applications. The characteristics which make these materials so attractive are their low density, high specific strength, good corrosion resistance, good workability, high thermal and electrical conductivity, and intrinsic recyclability. In the last two decades, the automotive industry<sup>1</sup> has increased the use of aluminum, and it will gain a central role in the rising market of electric vehicles.<sup>2,3</sup> Aluminum alloys are a perfectly suitable choice in the design of lightweight car bodies, with the aim of reducing fuel consumption, and in batteries manufacturing, where it is employed in producing electrodes, conductive busbars, hermetic enclosures, or structural packaging.<sup>4</sup>

Laser beam welding has established itself a solution for welding of aluminum, thanks to the fact that the beam has high energy density but deliver a low overall heat input. This allows the achievement of fine welding seam with narrow heat affected zone and very little thermal distortion.<sup>5,6</sup> However, laser beam welding has to deal with many issues that are connected with the properties of the processed material. First of all, the high reflectivity of aluminum and its alloys has been for years a major obstacle to the achievement of consistent laser welding results in terms of quality and productivity.

Nowadays, high-brilliance fiber lasers represent a key tool for industrial manufacturing in terms of wavelength and available power in continuous wave.<sup>7,8</sup> Welding in the keyhole regime<sup>9</sup> can be easily achieved, and it has the advantage to create a weld seam

with high aspect ratio (depth over width), limited heat affected zone, higher penetration, and good mechanical properties. On the other hand, the generated keyhole cavity is affected by instability which can lead to various defects like spatter<sup>10,11</sup> and pore formation.<sup>12–14</sup> Moreover, cracking<sup>15</sup> and loss of low vaporization temperature alloying elements are common events with detrimental effects on the mechanical properties.<sup>16</sup> To reduce or eliminate the occurrence of these defects is necessary to find optimal process parameters.<sup>17,18</sup> The most significant factors that play a role in laser welding are the laser power, the welding speed, the focal spot dimension, and, if present, the chemical composition of the shielding gas.<sup>19</sup> Their influence on the process result has been widely examined in the literature.

For quality assessment of the welds, process monitoring is a promising industrial solution that can be integrated in production systems with the aim of automatic detection of defective components. Various sensors are exploited for this purpose.<sup>20–22</sup> Radiation intensity detectors like photodiodes are a common choice,<sup>23,24</sup> they offer high temporal resolution and with appropriate filters can detect light at different wavelengths,<sup>25</sup> such as visible light, laser reflected radiation, or infrared.<sup>26</sup> Despite several efforts in the literature, the assessment of quality attributes along with the use of a noninvasive monitoring device able to detect such changes remains an open question. Indeed, in lap-joint welds with multiple layers, the monitoring needs increase due to the higher complexity of the joint.

Accordingly, the present study is aimed at autogeneous laser weldability study of 5754 Al-alloy in double lap-joint configuration in terms of process parameters and weld seams morphology. In parallel, the monitoring of the process back-reflected light is performed exploiting the in-source available monitoring system.

## II. MATERIALS AND METHODS

### A. Material

The investigated material is aluminum alloy 5754 (AlMg<sub>3</sub>) in the form of 1 mm thick sheets. The alloy is not heat-treatable and is characterized by a percentage of magnesium around 3% of the weight. It shows good weldability and formability together with good mechanical properties and good resistance to corrosion. It finds applications in vehicle bodies in automotive, shipbuilding, food processing equipment, and welded chemical and nuclear structures. The nominal ultimate tensile strength (UTS) of the material is in the range of 220–270 MPa. The chemical composition of the alloy is shown in Table I.

### B. Laser welding system

The laser welding system is composed of the laser source and the laser welding head containing the collimation and focusing lenses. The laser source is a high-brilliance 3 kW fiber laser

TABLE I. Nominal chemical composition of Al-alloy 5754.

Alloy	Si	Fe	Cu	Mn	Mg	Cr	Zn	Ti	Others
5754	0.40	0.40	0.10	0.50	2.60–3.60	0.30	0.20	0.15	0.05

TABLE II. Laser source specifications.

Specification	Symbol	Value
Emission wavelength	$\lambda$	1080 nm
CW emission power	$P$	3000 W
Beam quality	$M^2$	6.98
Beam parameter product	BPP	2.4 mm mrad

(nLIGHT alta™). The delivery fiber core diameter is 100  $\mu\text{m}$ . The laser is specifically designed to safely process highly reflective materials such as copper or aluminum. Internal hardware-based back reflection (BR) protection removes back-reflected light from the fiber and safely dissipates it as heat. The laser is also equipped with internal photodiode sensors that detect back-reflected laser light.

The analog output of these photodiodes can be externally read for real-time process monitoring.<sup>27</sup> The laser source specifications are shown in Table II.

The laser head is equipped with a 75 mm collimating and a 200 mm focal lens producing a theoretical spot size of 267  $\mu\text{m}$  on the focal plane (Laser Mechanisms FiberMINI). A cross-jet of compressed air is used to prevent optics to be damaged by fumes or spatter. The optical chain specifications and the resultant focal spot size are shown in Table III.

According to the caustic equation that describes the laser beam propagation, the diameter of the spot on the workpiece surface is computed even in defocused conditions. In the following equation, to compute the beam diameter at a given distance  $d(z)$ , the following are considered:  $d_0$  that represents the waist spot diameter,  $z_0$  which is the focal distance,  $z$  is the considered distance, thus  $z - z_0$  is the defocusing value, and  $\theta$  is the divergence angle,

$$d^2(z) = d_0^2 + (z - z_0)^2 \theta^2. \quad (1)$$

In order to comprehend the effect of focal position, the Rayleigh length  $z_r$  is a representative indicator. It describes the distance from the focal position, at which the beam diameter is enlarged by a factor of  $\sqrt{2}$ . Accordingly, the Rayleigh length is described as

$$z_r = \frac{\pi d_0^2}{4 M^2 \lambda}. \quad (2)$$

TABLE III. Optical chain specifications.

Specification	Symbol	Value
Collimation length	$f_{\text{col}}$	75 mm
Focal length	$f_{\text{foc}}$	200 mm
Fiber core diameter	$\Phi_{\text{core}}$	100 $\mu\text{m}$
Focal spot diameter	$d_0$	267 $\mu\text{m}$
Divergence angle	$\theta$	0.036 rad

The beam size at the Rayleigh length is, therefore,

$$d(z_r) = d_0\sqrt{2}. \quad (3)$$

The Rayleigh length of the optical configuration was calculated as 7.43 mm with a beam diameter of 0.378 mm at this length. Figure 1(a) represents the caustic shape of the beam according to Eq. (1) with the beam radius at the Rayleigh length highlighted. Figure 1(b) shows the acquired beam profile.

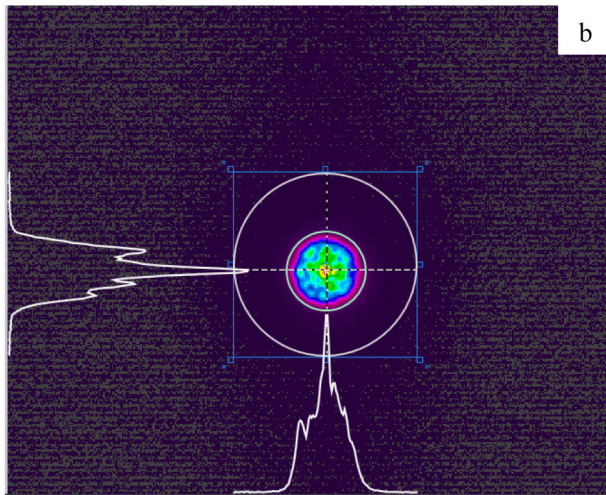
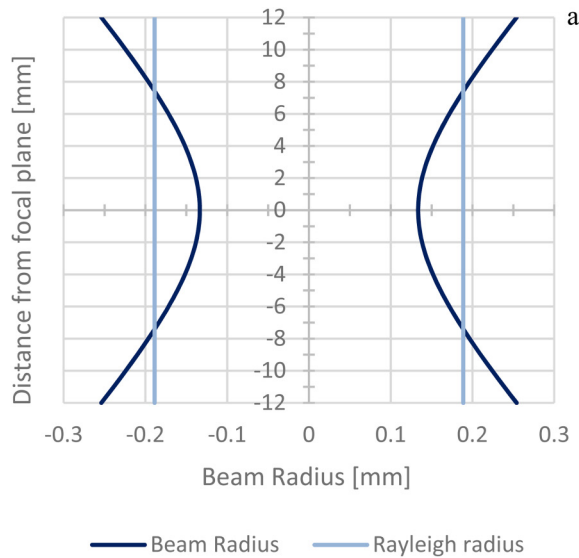


FIG. 1. (a) Calculated caustic shape of the laser beam and beam radius at Rayleigh length is highlighted. (b) Measured beam profile at the focal position.

TABLE IV. Fixed and variable parameters in the determination of process feasibility window.

Fixed parameters	Values
Power, $P$ (W)	3000
Optical magnification	2.67
Variable parameters	Values
Welding speed, $v$ (m/min)	From 1.2 to 14.2
Focal position, $f$ (mm)	0; -2; -4

### C. Characterization equipment

In order to obtain images of the cross sections of the weld seams, the samples were cut, ground, and polished with up to  $1\mu\text{m}$  diamond suspension. Optical microscopy was used to acquire images of the cross sections of the specimen (Leitz ERGOLUX 200).

## III. EXPERIMENT

### A. Determination of the feasibility window

Autogeneous welding of three sheets of 5754 Al-alloy in lap-joint configuration was performed with the aim to detect the boundaries of the process in terms of morphological characteristics of the weld seams. The welds were linear with a length of 100 mm. Considering the chosen application, the parameters with the higher influence on the process are power, welding speed, and focal position. In Table IV the values of the fixed and the variable parameters considered in determination of the feasibility window are shown. The laser power is set at 3 kW. The welding speed was chosen between the value of 1.2 and 14.2 m/min at 1 m/min increments. The focal position was investigated at 0 mm (focus on the workpiece surface), at -2 and -4 mm (inside the workpiece), remaining within the Rayleigh length at all conditions. No shielding gas was used in the experiments. The obtained welds were categorized qualitatively according to the weld seam appearance.

In Table V the values of spot diameter at the three different defocusing conditions are shown and the related value of irradiance computed as

$$I = \frac{P}{A}, \quad (4)$$

where  $P$  is the laser power and  $A$  is the spot area.

TABLE V. Laser beam spot dimension on the workpiece surface at different defocusing levels and related value of irradiance.

Focal position, $f$ (mm)	Spot diameter, $d$ (mm)	Irradiance, $I$ (W/cm <sup>2</sup> )
0	0.267	$5.36 \times 10^6$
-2	0.277	$4.99 \times 10^6$
-4	0.303	$4.15 \times 10^6$

The threshold value for irradiance that distinguishes between conduction welding process and deep penetration (keyhole) welding is found in the literature to be approximately  $10^6 \text{ W/cm}^2$  for lasers with wavelength around 1070 nm.<sup>28,29</sup> In all the focal position conditions, the value is above the threshold, deep penetration welding is expected.

### B. Monitoring

The employed laser source has the possibility to monitor back reflection signal directly from control interface connectors. This is because monitoring photodiodes are mounted inside the source to collect reflected radiation coming back from the process. The BR analog output has been connected with a shielded cable to a digital oscilloscope (Tektronix TBS-1042). The sampling rate was 1 kHz. The welding process was monitored in order to understand the capability of the BR signal to respond to different process conditions. Representative conditions for each qualitative category were identified, and three replicates were produced for acquiring monitoring signals.

## IV. RESULTS

### A. Process feasibility and weld bead types

Weld seams obtained at the different conditions of parameters were found to be crack-free and macrodefects were absent in their external appearance. Conditions at the highest level of defocusing and at the higher levels of welding speed showed a weak bonding of the third layer, which could be easily detached.

Due to machine dynamics, variation in the penetration was evident with respect to acceleration and deceleration. This phenomenon becomes more evident at higher welding speeds. The central and stationary section of the weld track is considered for the analysis of the results to remove these effects.

The welds obtained were categorized and analyzed according to morphological characteristics such as penetration, undercut, and the appearance of the bottom of the seam. The investigated process conditions are resumed in Table VI, the different colors represent the four macrocategories identified among the resultant weld seams. The first one (blue) is a full penetration condition that occurs at low speed and shows a weld with a wide groove, marked undercut and a droplike shape of the bottom seam. The second (yellow) is a full penetration condition with a narrow seam and less evident undercut, where the bottom side presents “icicle” structures. The third (orange) is a partial penetration condition, where the top surface is characterized by overfill. The fourth (red) is a partial penetration condition but the bond with the third layer is weak due to lack of penetration.

Cross sections of the welds at midtrack position were also acquired. Representative images for each category are presented in Table VII. As represented by the high aspect ratio (depth over width), it is possible to conclude that the welds are generated in keyhole regime. It can be seen that at low speed (first category) the weld is wide, with consistent undercut and dropout due to the metal flow through the bottom of the workpiece; pores and cavities are present. By increasing the speed (second category), the seam becomes narrower with reduced undercut and smaller pores.

TABLE VI. The morphological categorization of the weld seams.

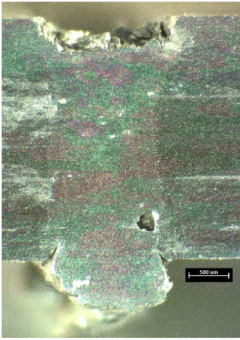
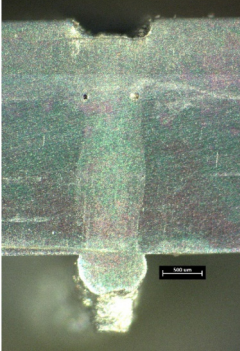
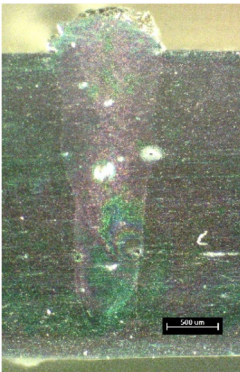
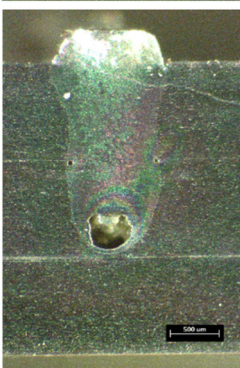
(1)	Drop-like bottom seam	
(2)	Icicles bottom seam	
(3)	Partial penetration	
(4)	Detachment of 3rd layer	

At high speed (third and fourth categories), penetration depth reduces until partial penetration condition, the weld is characterized by overfill and the diffused porosity is reduced but large pores are often present at the root.

For automotive applications, the second category is acceptable as it shows the full penetration with a simple visual inspection through the bottom side of the weld seam. The third category is promising as the weld shape and quality is superior; however, the penetration depth is not determined without a nondestructive inspection method. Indeed, the online monitoring signals can be useful for the purpose.

In order to have a comprehensive index that allow to compare different conditions taking into account the effect of laser power  $P$ , welding speed  $v$ , and spot diameter  $d$ , energy density is introduced.

TABLE VII. Cross section images for the different categories.

Category	Cross section	Process parameters
(1) Droplike bottom seam		Welding speed = 2.2 m/min, Focal position = 0 mm
(2) Icicles bottom seam		Welding speed = 8.2 m/min, Focal position = 0 mm
(3) Partial penetration		Welding speed = 11.2 m/min, Focal position = 0 mm
(4) Detachment of third layer		Welding speed = 11.2 m/min, Focal position = -4 mm

It is defined as

$$F = \frac{P}{v d}. \tag{5}$$

Figure 2 shows the experimented conditions and the corresponding quality categories of the obtained weld seams and the energy density index. It can be noticed that at high welding speed the energy density value varies in a narrow range and the effect of defocusing plays a significant role in the process outcome. Instead, in high heat input conditions, the energy density value grows faster with the decreasing of the speed and is much less sensitive to the focal position. This can lead to a state in which a robust process can be conducted at the lower speed allowed by quality and productivity constraints. Energy density appears to be a correct indicator to the change of processing conditions. The switches between categories appear to be approximately at 295, 70, and 50 J/mm<sup>2</sup> starting from the first category.

The energy density values in Fig. 2 can be useful for interpreting the formation mechanisms of the different weld seam categories. In first category conditions, there is a great quantity of energy delivered to the workpiece. A large keyhole forms piercing through the whole group of welded sheets, and since the speed is low, the molten material has time to flow through the bottom before solidifying. Pores are common in this type of weld due to the large amount of metal vapor generated, which remains entrapped in the turbulent flow of liquid during solidification. In the second category, the energy delivered to the piece is reduced as is the quantity of molten metal, which still can flow through the bottom. Due to the rapid solidification of the molten metal and the high melting point of aluminum oxide, the melt expulsion from the bottom of the weld seam occurs intermittently, generating the so-called icicles. The porosity is less because the keyhole is more stable at faster travel speeds.

In the third and fourth categories, the energy density is not high enough to produce full penetration welds; hence, the keyhole does not lead to an open end at the bottom. The motion of the

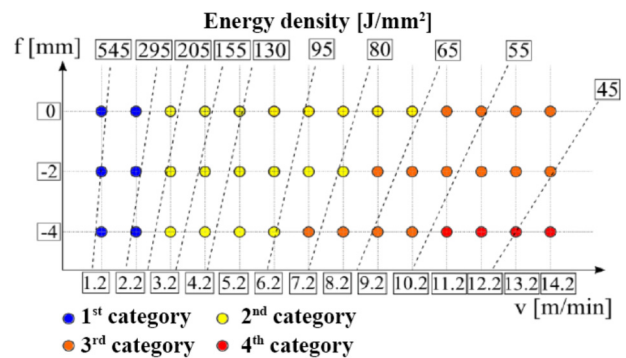


FIG. 2. The chart represents the process conditions, at different values of welding speed and defocusing, classified with respect to the weld type and the dashed lines identify the regions of the process that are at the same energy density level.

liquid metal in this case behaves differently, not being allowed to flow through the bottom, it tends to rise in the tail of the keyhole where solidification take place; therefore, a small amount of overfill is present. Root porosity is generated due to the fact that the entrapped vapor cannot easily escape from the bottom of the seam. The fourth category occurs when both energy density and irradiance levels are low, losing the penetration between the second and third plates. This underlines the importance of irradiance for initiating a sufficiently stable keyhole along with the energy density in order to penetrate deeper into the workpiece.

### B. Monitoring signal behavior

To verify the capacity of the monitored back reflection signal for identifying the different process categories and its possible variations, each experiment was monitored. The laser radiation, after the keyhole generation, rebounds inside it and is partly absorbed by the material and partly reflected outward. A portion of the reflected laser beam intercepts the optical path of the incoming beam and is launched back through the delivery fiber. The recorded signals for a representative condition of each morphological weld category are presented in Figs. 3–6. No postprocessing was done on the signals, and they represent the entire time history of the tracks.

It can be noticed from a visual comparison of the signal with the bottom of the seam, especially in high-speed welds, that the initial and final transients of axis acceleration and deceleration visible on the sample are clearly identified through the monitoring

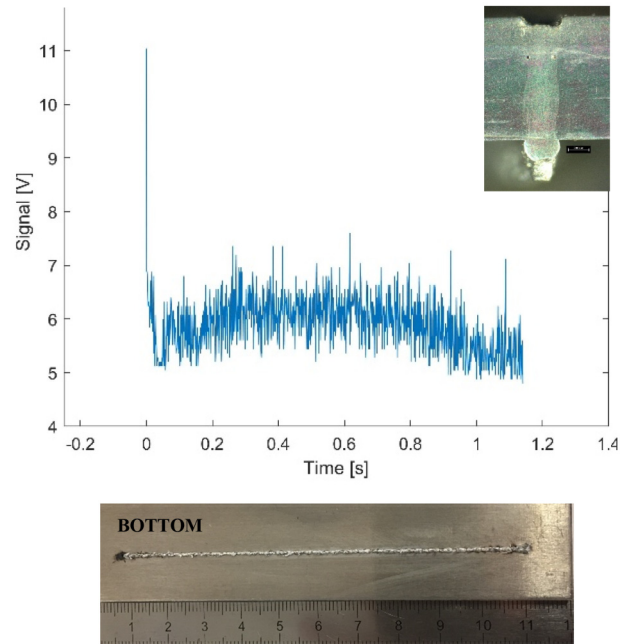


FIG. 4. Representative back reflection signal of second category acquired during process compared with the bottom seam. Welding speed = 8.2 m/min and focal position = 0 mm.

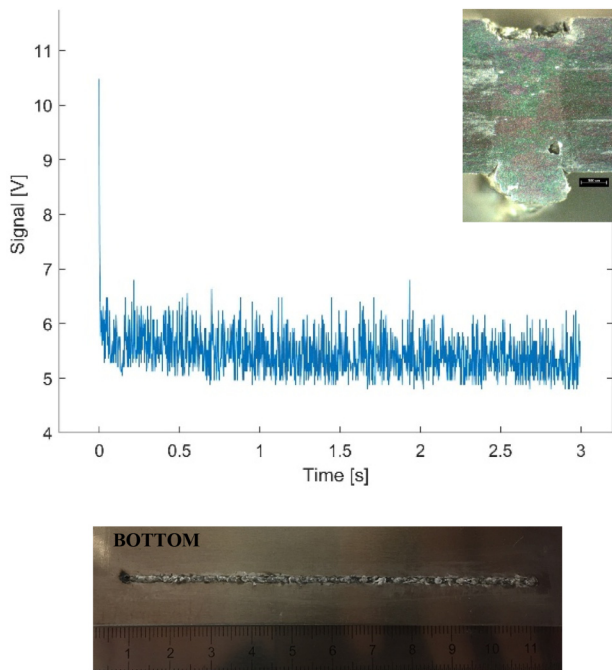


FIG. 3. Representative back reflection signal of first category acquired during process compared with the bottom seam. Welding speed = 2.2 m/min and focal position = 0 mm.

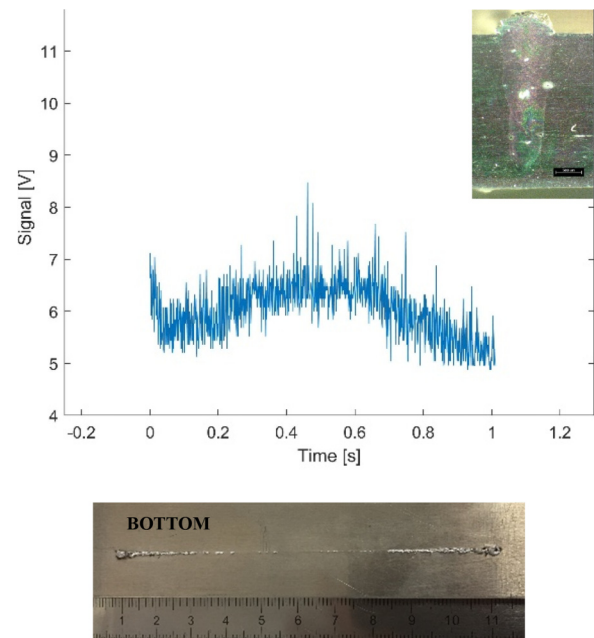
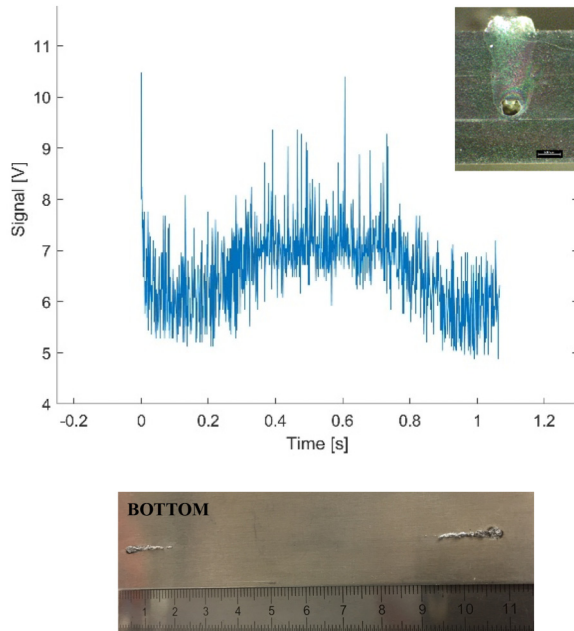


FIG. 5. Representative back reflection signal of third category acquired during process compared with the bottom seam. Welding speed = 11.2 m/min and focal position = 0 mm.



**FIG. 6.** Representative back reflection signal of fourth category acquired during process compared with the bottom seam. Welding speed = 11.2 m/min and focal position = -4 mm.

signal. In the stationary part of the process, the signal also maintains its mean value constant. A preliminary analysis was carried out to compare the signal mean value of the four weld categories, only the central part of them was selected.

In Fig. 7, the mean value of the signals and the corresponding penetration depth  $d_p$  are reported. It can be noticed that the signal

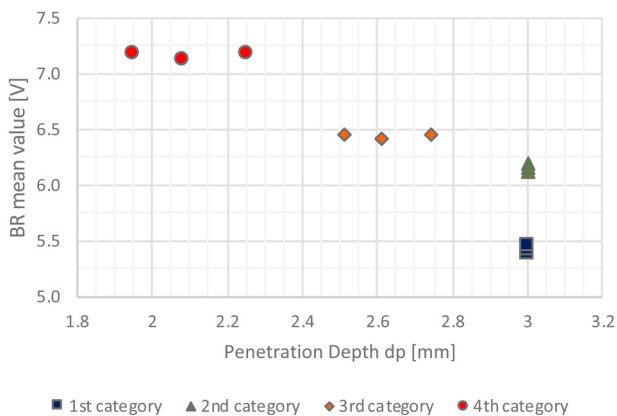


**FIG. 7.** BR mean value of the stationary process with respect to the penetration depth of the three replicates performed on the representative condition per each category.

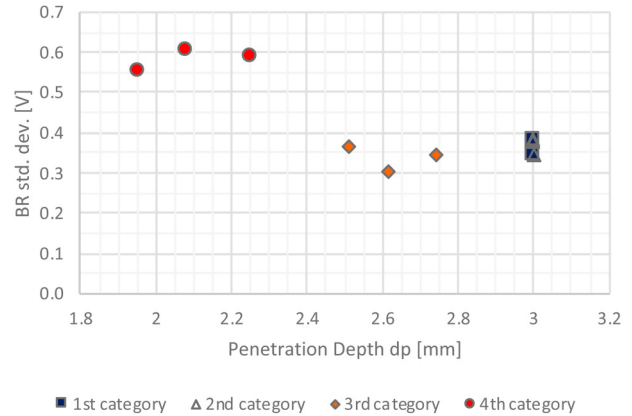


**FIG. 8.** BR standard deviation of the stationary process with respect to the penetration depth of the three replicates performed on the representative condition per each category.

strength is correlated to the weld penetration. The transition from full (first and second categories) to partial penetration (third and fourth categories) implies that some of the radiation is no longer able to escape from the bottom of the weld from the opening of the keyhole and more is reflected back.<sup>30,31</sup> Moreover, the signal strength further increases when the weld penetration is between the second and third sheets, thus passing from second to first category.

Moreover, the results show that in first and second categories, which are both characterized by full penetration, signal strength is remarkably different. In the first category, the amount of reflected radiation is lower, and this can be explained considering the keyhole dimension and the penetration capability. The keyhole is reasonably straight and wide due to the low speed, and the radiation is mainly absorbed by the material until it can travel through the piece. The remainder is expected to escape from the bottom end. In the second category, due to the increased welding speed, the keyhole is narrower and more inclined. Thus, a higher amount is back-reflected.

The standard deviation was also calculated for the stationary part of the signals and is reported in Fig. 8. It seems to remain almost constant except for the lack of penetration condition with -4 mm focal position, where it increases significantly. This is likely related to a higher instability of the keyhole at a lower level of irradiance.

It is possible to conclude that the monitored signal shows a promising capability to identify different welding conditions and process variations.

## V. CONCLUSION

This work investigated autogeneous laser beam welding of aluminum alloy 5754. The first step aimed at process comprehension with the detection of a feasibility region in which the variable factors chosen were welding speed and focal position. The obtained results were classified using a qualitative approach to discriminate different weld seam conditions. Four morphological categories were selected:



- (1) Welds in full penetration at low speed with wide groove and marked undercut on the top surface and droplike aspect on the bottom.
- (2) Welds in full penetration at moderate speed with narrow seam, little undercut, and icicles on the bottom.
- (3) Welds in partial penetration at high speed with overfill on the top.
- (4) Welds in partial penetration at high speed and focal position at  $-4$  mm, where detachment of the third sheet occurs.

The process categories were also identified by their value of energy density index that shows higher sensitivity to defocusing when welding speed is high. The process was less perturbed at lower speed.

The performed monitoring activity exploited the capability of an in-source monitoring system able to detect back-reflected radiation. The mean value of the stationary part of the signals was used to discriminate the different process conditions and to compare them, highlighting how the phenomena taking place during the process influence the outcomes in terms of morphology. The standard deviation of the back reflection was also computed, and it resulted effective to identify process disturbances related to defocusing. The signals show a promising capability to follow the variations in the resulting welds. Future works will investigate the relationship between the monitoring signals and the weld geometry, as well as its strength.

## REFERENCES

- <sup>1</sup>K. Hong and Y. C. Shin, "Prospects of laser welding technology in the automotive industry: A review," *J. Mater. Process. Tech.* **245**, 46–69 (2017).
- <sup>2</sup>G. Barbieri, F. Cognini, M. Moncada, A. Rinaldi, and G. Lapi, "Welding of automotive aluminum alloys by laser wobbling processing," *Mater. Sci. Forum* **879**, 1057–1062 (2017).
- <sup>3</sup>S. Ramasamy and C. E. Albright, "CO<sub>2</sub> and Nd-YAG laser beam welding of 5754-O aluminium alloy for automotive applications," *Sci. Technol. Weld. Joi.* **6**(3), 182–190 (2001).
- <sup>4</sup>G. Shannon and H. Chen, "Laser welding of aluminum and copper for battery welding applications using a 500 W single mode fiber laser," in *International Congress on Applications of Laser and Electro-optics (ICALEO)*, Orlando, FL, 3–6 November 2009 (Laser Institute of America, 2009), pp. 1015–1020.
- <sup>5</sup>X. Zhang, T. Huang, W. Yang, R. Xiao, Z. Liu, and L. Li, "Microstructure and mechanical properties of laser beam-welded AA2060 Al-Li alloy," *J. Mater. Process. Tech.* **237**, 301–308 (2016).
- <sup>6</sup>D. Narsimhachary, R. N. Bathe, G. Padmanabham, and A. Basu, "Influence of temperature profile during laser welding of aluminum alloy 6061 T6 on microstructure and mechanical properties," *Mater. Manuf. Process.* **29**, 948–953 (2014).
- <sup>7</sup>S. Katayama, H. Nagayama, M. Mizutani, and Y. Kawahito, "Fibre laser welding of aluminium alloy," *Weld. Int.* **23**(10), 744–752 (2009).
- <sup>8</sup>J. Corrado, S. Meco, S. Williams, and S. Ganguly, "Fundamental understanding of the interaction of continuous wave laser with aluminium," *Int. J. Adv. Manuf. Technol.* **93**, 3165–3174 (2017).
- <sup>9</sup>G. Xu and Z. Cheng, "Laser keyhole welding on aluminum alloys," *Proc. SPIE* **3888**, 710–716 (2000).
- <sup>10</sup>B. Chang, J. Blackburn, C. Allen, and P. Hilton, "Studies on the spatter behaviour when welding AA5083 with a Yb-fibre laser," *Int. J. Adv. Manuf. Technol.* **84**, 1769–1776 (2016).
- <sup>11</sup>F. Caiazzo, V. Alfieri, F. Cardaropoli, and V. Sergi, "Characterization of lap joints laser beam welding of thin AA 2024 sheets with Yb:YAG disk-laser," *Proc. SPIE* **8433**, 84330Z (2012).
- <sup>12</sup>A. C. Popescu, C. Delval, and M. Leparoux, "Control of porosity and spatter in laser welding of thick AlMg5 parts using high-speed imaging and optical microscopy," *Metals* **7**(11), 452 (2017).
- <sup>13</sup>N. Seto, S. Katayama, and A. Matsunawa, "Porosity formation mechanism and suppression procedure in laser welding of aluminium alloys," *Weld. Int.* **15**(3), 191–202 (2001).
- <sup>14</sup>Y. Yu, C. Wang, X. Hu, J. Wang, and S. Yu, "Porosity in fiber laser formation of 5A06 aluminum alloy," *J. Mech. Sci. Technol.* **24**, 1077–1082 (2010).
- <sup>15</sup>X. Wang, F. Lu, H. Wang, H. Cui, X. Tang, and Y. Wu, "Mechanical constraint intensity effects on solidification cracking during laser welding of aluminum alloys," *J. Mater. Process. Tech.* **218**, 62–70 (2015).
- <sup>16</sup>X. Cao, W. Wallace, J. Immarigeon, and C. Poon, "Research and progress in laser welding of wrought aluminum alloys. II. Metallurgical microstructures, defects, and mechanical properties," *Mater. Manuf. Process.* **18**(1), 23–49 (2003).
- <sup>17</sup>X. Cao, W. Wallace, C. Poon, and J. Immarigeon, "Research and progress in laser welding of wrought aluminum alloys. I. Laser welding processes," *Mater. Manuf. Process.* **18**(1), 1–22 (2003).
- <sup>18</sup>B. Hu and B. H. M. Richardson, "Autogenous laser keyhole welding of aluminium alloy 2024," *J. Laser Appl.* **16**, 70–80 (2005).
- <sup>19</sup>M. Jiang, W. Tao, S. Wang, L. Li, and Y. Chen, "Effect of ambient pressure on interaction between laser radiation and plasma plume in fiber laser welding," *Vacuum* **138**, 70–79 (2017).
- <sup>20</sup>D. Y. You, X. D. Gao, and S. Katayama, "Review of laser welding monitoring," *Sci. Technol. Weld. Joi.* **19**(3), 181–201 (2014).
- <sup>21</sup>J. Stavridis, A. Papacharalampopoulos, and P. Stavropoulos, "Quality assessment in laser welding: A critical review," *J. Adv. Manuf. Technol.* **94**, 1825–1847 (2018).
- <sup>22</sup>S. H. Lee and J. Mazumder, "Spectroscopic measurements of plasma plume for welding monitoring," in *ICALEO 2009: 28th International Congress on Laser Materials Processing, Laser Microprocessing and Nanomanufacturing, Orlando, FL, 3–6 November 2009* (Laser Institute of America, 2009), pp. 638–644.
- <sup>23</sup>A. F. H. Kaplan, P. Norman, and I. Eriksson, "Analysis of the keyhole and weld pool dynamics by imaging evaluation and photodiode monitoring," in *Proceedings of LAMP2009—the 5th International Congress on Laser Advanced Materials Processing, Kobe, Japan, 29 June–2 July 2009* (Sumitomo Corp., Tokyo, 2009), pp. 1–6.
- <sup>24</sup>F. Bardin *et al.*, "Optical techniques for real-time penetration monitoring for laser welding," *Appl. Opt.* **44**, 3869–3876 (2005).
- <sup>25</sup>P. De Bono *et al.*, "Welding Investigation of optical sensor approaches for real-time monitoring during fibre laser welding," *J. Laser Appl.* **29**, 22417 (2017).
- <sup>26</sup>J. Yu, Y. Sohn, Y. Whan, and J. Kwak, "The development of a quality prediction system for aluminum laser welding to measure plasma intensity using photodiodes," *J. Mech. Sci. Technol.* **30**, 4697–4704 (2016).
- <sup>27</sup>D. A. V. Kliner, "nLIGHT alta™: A Versatile, Next-Generation Fiber Laser Platform for kW Materials Processing," in *Proceedings of the 84th Laser Materials Processing Conference, Nagoya, Japan, January 2016* (Japan Laser Processing Society, Nagoya, 2016).
- <sup>28</sup>H. Zhao, D. R. White, and T. Debroy, "Current issues and problems in laser welding of automotive aluminium alloys," *Int. Mater. Rev.* **44**(6), 238–266 (1999).
- <sup>29</sup>K. H. Leong, K. R. Sabo, P. G. Sanders, and W. J. Spawr, "Laser welding of aluminum alloys," *Proc. SPIE* **2993**, 37–45 (1997).
- <sup>30</sup>D. You, X. Gao, and S. Katayama, "Multiple-optics sensing of high-brightness disk laser welding process," *NDT E Int.* **60**, 32–39 (2013).
- <sup>31</sup>K. Kamimuki, T. Inoue, K. Yasuda, M. Muro, T. Nakabayashi, and A. Matsunawa, "Behaviour of monitoring signals during detection of welding

defects in YAG laser welding. Study of monitoring technology for YAG laser welding (Report 2)," *Weld. Int.* 17(3), 203–210 (2003).

### Meet the Authors

Matteo Garavaglia received his BSc in mechanical engineering from Politecnico di Milano, Italy, in 2015. He gained his MSc in mechanical engineering with a specialization in advanced materials and manufacturing track in 2018. He developed his MSc thesis work at SITEC—Laboratory for Laser Application in cooperation with Optoprim srl and the technical support of nLIGHT Inc. The field of study regards laser processes, in particular, high-brilliance fiber laser welding and monitoring.

Ali Gökhan Demir was born in Istanbul, Turkey, in 1985. He received his MSc in mechanical engineering and European Ph.D. degree in mechanical engineering from the Politecnico di Milano, Italy, in 2009 and 2014, respectively. He has been Assistant Professor with the Department of Mechanical Engineering, Politecnico di Milano, since 2015. He has authored over 50 papers in international journals and international conference proceedings. His current research interests include laser-based manufacturing processes, mainly, additive manufacturing, laser micromachining, and process monitoring with the SITEC—Laboratory for Laser Applications.

Stefano Zarini received his MSc and Ph.D. in mechanical engineering from the Politecnico di Milano in 2012 and 2016,

respectively. His Ph.D. work involved the development of a real-time process control system for laser metal deposition (LMD). Since 2016, he is with Optoprim srl developing laser-based manufacturing processes and systems for cladding, cutting, welding, and heat treatment operations.

Brian Victor is Director of Industrial Applications for nLIGHT Inc. in Vancouver, Washington, USA. Brian supports nLIGHT's fiber laser customers and applications partners by developing laser processing solutions and troubleshooting manufacturing challenges. Brian holds BS and MS degrees in welding engineering and has developed laser process expertise in welding, cutting, cladding, brazing, and heat treating for a variety of markets and material systems.

Barbara Previtali received the Ph.D. degree in manufacturing and production system from the Politecnico di Milano, Milan, Italy, in 2002. In 2016, she was appointed as Full Professor in the Mechanical Engineering Department, Politecnico di Milano. She leads the SITEC—Laboratory for Laser Applications and PromozioneL@ser with AITeM, which collects Italian laser users in industry and academia. Her current research interests include modeling, optimization, and control of laser processes in their application in various fields. On these research subjects, she has authored or co-authored over 100 papers in refereed international journals and international conferences and two international patents.